$\mathcal{H}_\infty$ Control for the PACOSS DTA*

Christopher T. Voth† and R. Michael Stoughton

Research and Technology Department
Martin Marietta Civil Space Company

Abstract

This paper presents an application of an $\mathcal{H}_\infty$ design technique to the active control of a passively damped large space structure test article. An active vibration suppression compensator was designed for the Passive and Active Control of Space Structures (PACOSS) Dynamic Test Article (DTA) using the $\mathcal{H}_\infty$ technique. Analytic studies indicate passive damping of the structure results in reduced sensitivity to variations in plant structural modes for a given level of performance.

The control problem was to reduce the X and Y Line-of-Sight (LOS) pointing errors caused by deformation of the structure due to vibration. External disturbances at four locations along the DTA excite the vibrational modes of the structure, resulting in LOS errors. Passive damping elements designed into the structure result in open-loop damping ratios ranging from 0.12 to 0.02. Active suppression of structural modes is accomplished using 10 proof-mass actuators located on the structure. Sensors for active control provide 20 colocated inertial and relative velocity measurements as well as 3 noncolocated inertial velocity measurements at locations along the structure.

The $\mathcal{H}_\infty$ approach allowed the integration of performance requirements, robustness requirements, and other design constraints into the design problem. Explicit representation of model uncertainties was important in achieving a closed-loop system insensitive to plant variations typical of flight hardware.

Implementation of the resulting controller on the DTA structure provided experimental verification of closed-loop system stability and performance in the presence of model errors typical of test verified structures possessing high modal density.

An investigation of the relationship between the active control and passive damping indicated that passive damping was instrumental in achieving performance and reduced sensitivity to structural mode uncertainty. Passive damping of the structure also aided in reduction of the controller order for hardware implementation.

*Performed under Air-Force contract F33615-82-C-3222

†P.O. Box 179, Denver, Colorado 80201, (303) 977-4164

1 Introduction

Future scientific, commercial and military objectives in space will require construction of Large Space Systems (LSS). Proposed operational performance objectives for these large structures include stringent pointing accuracies, fast repositioning and short settling times. LSS will necessarily be lightweight and exhibit a dense, low-frequency modal spectrum with significant content within the control bandwidth.

Passive and active control methods will likely play important roles in achieving performance requirements for future LSS missions. The complexity of LSS structural dynamics often result in significant model inaccuracies. Attempts to control similar large systems through purely active means have often produced disappointing results.

The Dynamic Test Article (DTA) is a ground test experiment designed and built as part of the Passive and Active Control of Space Structures (PACOSS) program. The PACOSS program was initiated to investigate solutions to control-structure interaction problems by combining passive damping approaches, designed into the structure, with active control. The DTA was designed as a hardware validation experiment to simulate a large pointing system and contains seven substructures representative of future LSS.

This report describes the application of the $\mathcal{H}_\infty$ design method to the active control of the DTA large space structure experiment. Passive damping elements designed into the structure provide increased open-loop structural damping and vibration suppression. Active control is used to futher reduce pointing errors due to vibrations present in the passively damped DTA structure.

The $\mathcal{H}_\infty$ approach allowed integration of performance requirements, robustness requirements, and other design constraints into the design problem. Representations of model uncertainty are used to reduce the sensitivity of the closed-loop design to model inaccuracies. Uncertainties within the control bandwidth prevent the cancellation of plant dynamics by compensator zeros, resulting in a design which is less sensitive to model errors. The resulting design is less sensitive to model errors typical of flight hardware.

Implementation of the active controller on the DTA structure provided experimental verification of closed-loop system stability and performance in the presence of model errors typical of test verified structures with high modal density. Tests results are given in the form of frequency responses and time response functions and show good agreement to analytic predictions for the final design.

An analytical study was performed to investigate the relationship between the active control and passive damping. Results indicate that passive damping was instrumental in achieving performance and reduced sensitivity to structural mode uncertainty. Passive damping of the structure also aided in reduction of the controller order for hardware implementation.

The algorithm used to solve the $\mathcal{H}_\infty$ control problem is from the MATLAB *Robust Control Toolbox* and is described in Reference [4]. An excellent tutorial description and overview of $\mathcal{H}_\infty$ based control design is provided by Maciejowski [3].

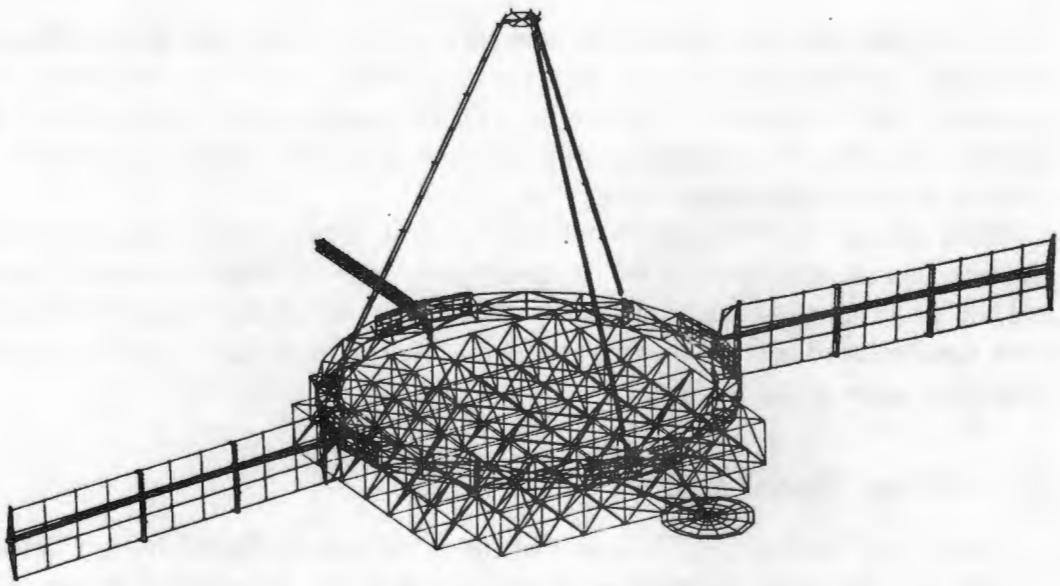

Figure 1: Dynamic Test Article

2 PACOSS Dynamic Test Article (DTA)

Figure 1 is a picture of the DTA. The DTA is a ground based structure for experimental validation of control design approaches applicable to LSS. The DTA is designed to simulate a large pointing system. The control objective is to minimize the effect of disturbances on the pointing accuracy of the structure. The pointing accuracy is defined in terms of the relative alignment of selected points on the lower truss structure and the secondary mirror structure on top of the tripod. The DTA is composed of 7 substructures which represent the following real structures: the lower ring truss represents a structural 'hardback' for the system. The lower box truss structure is a support structure intended for a large primary optical surface. The tripod system is intended to support a secondary mirror. The dish antenna is a communications antenna and the linear truss is to support sensitive equipment. Large side-panels represent two solar arrays.

2.1 Dynamic Description of DTA

The structure is symmetric about an axis running between the dish antenna and the linear truss and contains 39 modes below 10 Hz. Of these modes 6 are associated with the suspension mechanism for supporting the structure, 10 are associated with the actuators (each actuator is modeled as a 2^{nd} order system), and 23 are structural modes. Many higher frequency structural modes exist in the system which are not included in the model. The structure was designed with passive damping elements to provide increased damping of the structural modes. Damping ratios of the structural modes range from 0.01 to 0.12. Similar large structures without passive damping have damping ratios less than 0.01.

The 10 actuators are proof-mass actuators, with a $\pm$ 1.0 inch stroke. Two actuators are located on the tripod, six on the lower ring truss structure and two on the box truss structure. These actuators work well for vibration suppression; however since they rely on the acceleration of a sliding mass to generate actuation force, they are only effective within a bandpass frequency range.

Each actuator has two sensors colocated with it. One is and accelerometer, filtered to measure inertial velocity, and the other measures relative velocity between the structure and the proof-mass of the actuator. In addition to the 20 colocated sensors, there are three noncolocated accelerometers with ouput filtering to measure inertial velocities, one located on each of the two solar arrays, and one on the linear truss.

2.2 Linear Model of DTA

A Linear Time-Invariant (LTI) model of the DTA was developed from a finite element analysis and verified with extensive modal testing of the assembled structure. The model formed the basis for the controller design and is more accurate than would typically be available for flight hardware.

The DTA structure contains modes beyond 10 Hz which have been truncated from the model. In addition to the sensor outputs, the model has two design outputs. The design outputs are X and Y axis Line-of-Sight (LOS) pointing errors. The LOS outputs are measurements of the relative alignment between the lower optical surface and the secondary mirror structure. The Y axis error is measured along an axis aligned with the axis of symmetry of the structure. The X axis error is measured relative to an axis perpendicular to the Y axis and passing through the center of the solar array panels.

Vibrational modes of system are excited by 4 disturbance inputs located on the box truss structure. Of the 23 structural modes, only 12 affect the sensor measurement outputs or the LOS outputs. The model used in the active control design contained only 12 structural modes and had a total of 28 dynamic modes.

Figure 2 shows the maximum singular value of the DTA model frequency response from the 4 disturbance inputs to each of the X and Y LOS errors. The effect of passive damping elements on vibration suppression is apparent from these plots. Few sharp resonant peaks characteristic of the response of an undamped structure are present.

3 Design Problem

The design problem facing the control engineer can be described as achieving the best trade-off between a set of performance requirements, design constraints, and sensitivity of the system to model uncertainties. The primary performance requirement for the closed-loop system is to minimize the relative LOS error in both the X and Y axes resulting from disturbances. Disturbances acting on the structure are in the frequency range from 1–10 Hz.

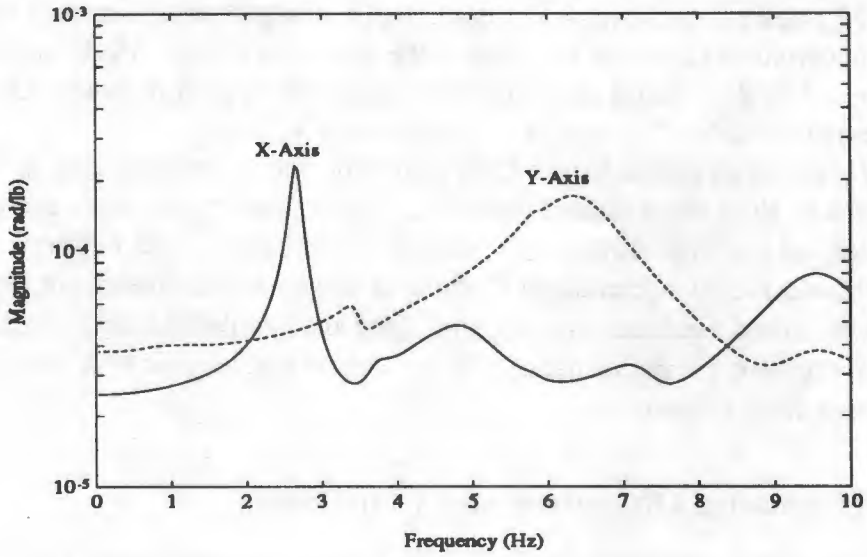

Figure 2: Maximum Singular Values of the Response from the Disturbance Inputs to the X and Y Axis LOS Errors for the DTA Model.

Design constraints and model uncertainties are:

- actuator displacement limited to ± 1.0 inches,
- unmodeled high frequency modes above 10 Hz,
- 5% uncertainty in structural mode frequency,
- 20% uncertainty in structural mode damping,

Additional constraints are related to the implementation of the controller. The controller must be digitally implemented at a sample rate of 280 Hz. The maximum size of the compensator is limited to 58 states.

4 Synthesis Model

Multivariable control design with modern techniques involves formulation of design performance objectives and other requirements in the form of a *synthesis model*. The synthesis model includes the model of the plant dynamics with control inputs and sensor outputs along with additional inputs and outputs which are important in the design. Design weighting functions on selected plant inputs and outputs are augmented with the plant model to form the synthesis model.

With $\mathcal{H}_\infty$ design, performance requirements, design constraints and representations of model uncertainties must be included in the synthesis model. Model uncertainties may be represented as $\mathcal{H}_\infty$ -norm criteria based on the small gain theorem. Development of the synthesis model for $\mathcal{H}_\infty$ design is discussed by Boyd [1].

The $\mathcal{H}_\infty$ synthesis model for the DTA control design is a transfer matrix represented by $P(s)$. Inputs to $P(s)$ are separated into a vector of control inputs, $u(s)$, and the exogenous input vector, $w(s)$. The vector $w(s)$ includes disturbances, and fictitious design inputs for representing model uncertainty. Outputs of the synthesis model are separated into a vector of measured feedback signals, $y(s)$, and the regulated output vector, $z(s)$. The vector $z(s)$ contains the performance criteria outputs and outputs which define constraints on the closed-loop system.

4.1 Performance Objectives and Constraints

The primary performance requirement for the DTA is to minimize the LOS error resulting from the external disturbances. This can be expressed as minimizing

$$\overline{\sigma}[H_{e_{LOS}d}(j\omega)]. \tag{1}$$

where:

$H(s)$	is the closed-loop transfer matrix of the plant and controller,
e_{LOS}	is an output vector containing X and Y LOS errors,
d	is a vector of disturbance inputs,
$\overline{\sigma}[\,]$	signifies the maximum singular value.

The performance criteria may be represented as a weighting function $W_S(s)$ on the design output $e_{\mathrm{LOS}}(s)$. Let $W_S(s)$ be a diagonal transfer function matrix:

$$W_S(s) = \begin{bmatrix} w_{s_x}(s) & 0 \\ 0 & w_{s_y}(s) \end{bmatrix} \tag{2}$$

where:

$w_{s_x}(s)$	is a transfer function weighting for X axis LOS error,
$w_{s_y}(s)$	is a transfer function weighting for Y axis LOS error.

The $\mathcal{H}_\infty$ design criteria for performance is to find a controller such that:

$$||W_S(s)H_{e_{\mathrm{LOS}}d}(s)||_\infty < 1. \tag{3}$$

which implies:

$$\overline{\sigma}[H_{e_{\mathrm{LOS}_X}d}(j\omega)] < |w_{s_x}^{-1}(j\omega)| \tag{4}$$

$$\overline{\sigma}[H_{e_{\mathrm{LOS}_Y}d}(j\omega)] < |w_{s_y}^{-1}(j\omega)| \tag{5}$$

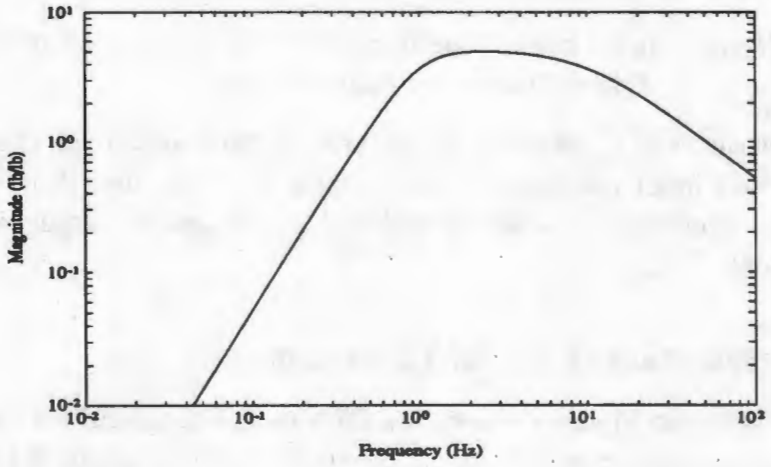

Figure 3: Magnitude plot of $w_{r_i}^{-1}$ weighting functions.

where:

e_{LOS_X} is the X axis LOS error,
e_{LOS_Y} is the Y axis LOS error.

By reducing $|w_{s_x}^{-1}(s)|$ and $|w_{s_y}^{-1}(s)|$ one can find the controller which minimizes the LOS error.

A constraint on actuator control activity is included in the synthesis model by limiting the closed-loop response from disturbances $d(s)$ to the controller output $u(s)$. The proof-mass actuators are only capable of providing force over a limited bandwidth. To account for this physical constraint, the closed-loop response is restricted to be 'band-pass' over the effective frequency range of the actuators. This is accomplished through the weighting function $W_R(s)$ on the closed-loop control vector $u(s)$.

$$W_R(s) = \begin{bmatrix} w_{r_1}(s) & & 0 \\ & \ddots & \\ 0 & & w_{r_{10}}(s) \end{bmatrix} \tag{6}$$

where:

$w_{r_i}(s)$ is a transfer function weighting on the i^{th} controller output.

In theory each of the controller outputs could be individually weighted. As a simplification an identical weighting is used on each of the outputs. Figure 3 is a plot of the magnitude of the $w_{r_i}^{-1}$ transfer functions.

The $\mathcal{H}_\infty$ design constraint is to find a controller such that:

$$||W_R(s)H_{ud}(s)||_\infty < 1. \tag{7}$$

where:

$H_{ud}(s)$ is the closed loop transfer matrix from the disturbance input vector d, to the controller output vector u.

The disturbances $d(s)$ form the design criteria input vector $w_c(s)$ which is included in the exogenous input vector $w(s)$. The outputs of $W_S(s)$ and $W_R(s)$ form the design criteria output vector $z_c(s)$ which is included in the design output vector $z(s)$ of the synthesis model.

4.2 Representation of Model Uncertainty

The block diagram in Figure 4 shows the DTA model separated into a ladder structure. Model uncertainties are represented by Δ blocks at several locations in the nominal model. The block Δ_{add} represents unmodeled high frequency (>10 Hz) structural dynamics in the form of an additive uncertainty across the plant. The legend of Figure 4 indicates the types of uncertanties represented by each of the Δ blocks.

DTA model uncertainties shown in Figure 4 must be represented in the synthesis model. Model uncertainties may be represented as $\mathcal{H}_\infty$ -norm criteria based on the small gain theorem. Uncertainties shown in Figure 4 may be grouped into a single block diagonal structure represented by $\mathbf{\Delta}(s)$. The uncertainty block $\mathbf{\Delta}(s)$ is normalized by scaling gains at the plant inputs and outputs such that

$$||\mathbf{\Delta}(s)||_\infty < 1. \tag{8}$$

Figure 5 is a block diagram showing the relationship between the synthesis model $P(s)$, the block-diagonal uncertainty matrix, $\mathbf{\Delta}(s)$ and the controller $F(s)$. The input vector z_Δ to Δ is included in the z vector of regulated outputs of the synthesis model. The output vector w_Δ to Δ is part of the exogenous input vector, w, of the synthesis model. From the 'small gain theorem' if a controller is found such that

$$||H_{zw}(s)||_\infty < 1, \tag{9}$$

where:

H_{zw} is the closed-loop transfer matrix from w to z,

then the closed loop system will be stable for all possible plant variations represented by $\mathbf{\Delta}$. Maciejowski [3] and Doyle [2] provide more detail in modeling of uncertainty and representation by the small gain theorem.

The synthesis model for the DTA contains a simpler set of plant uncertainties than shown in Figure 4. This simplification is motivated by the overconstrained nature of the complete $\mathcal{H}_\infty$ design problem. The $\mathcal{H}_\infty$ problem results in a closed-loop system with

$$||H_{zw}(s)||_\infty < 1. \tag{10}$$

By using the $\mathcal{H}_\infty$ norm from w to z as the design criteria, the diagonal structure of $\mathbf{\Delta}$ is ignored. The uncertainty Δ is taken to be a fully coupled matrix. As the size of

Legend: Plant Model	
$\{A_i, B_i, C_i\}$:	state-space representation of ith structural mode
e_{LOS}:	X and Y LOS errors
y:	sensor output vector
u:	controller output vector
d:	disturbance input vector

Legend: Uncertainties	
Δ_{add}:	unmodeled structural modes
Δ_{A_i}:	actuator modal displacement for ith mode
Δ_{S_i}:	sensor modal displacement for ith mode
Δ_{F_i}:	pole locations for ith mode

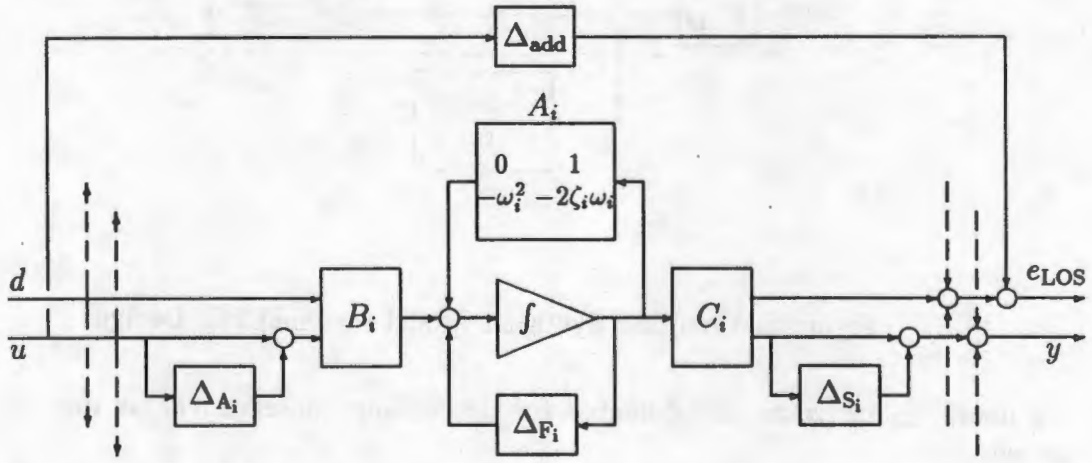

Figure 4: Block Diagram of the DTA Plant Model Showing Representation of Uncertainty.

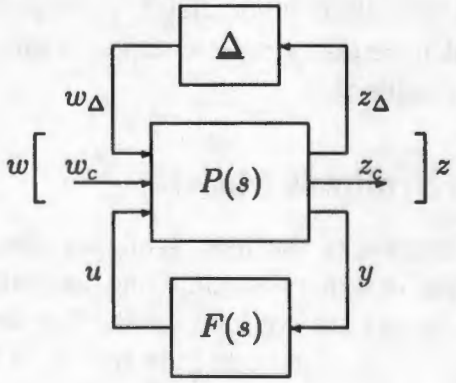

Figure 5: Closed-loop system of synthesis model and controller.

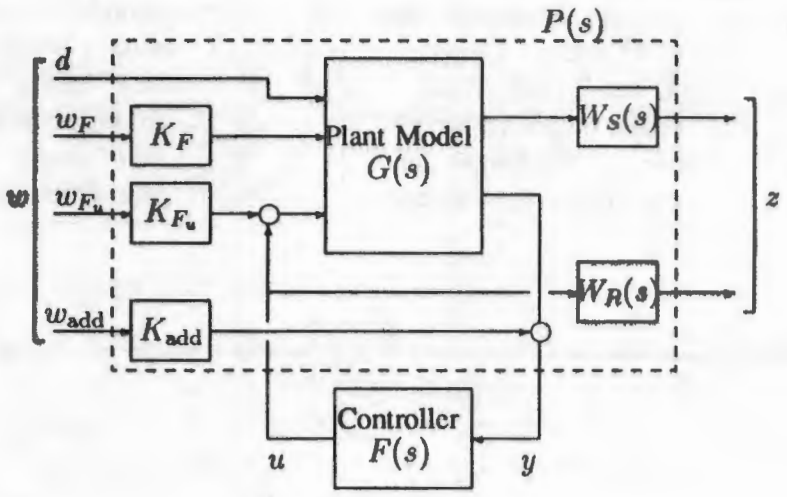

Figure 6: Complete Synthesis Model for Final $\mathcal{H}_\infty$ Design

the matrix Δ increases, the potential for introducing conservativeness into the design increases.

An initial control design for the DTA used a synthesis model which did not include the plant model pole uncertainties represented by Δ_{F_i}. This initial design was found to be sensitive to variations in the plant dynamics. The initial control design was particularly sensitive to the 18th and 19th design model structural mode pole locations. Addition of a feedback uncertainty representation Δ_{F_u} from the LOS error outputs to the control inputs reduced the sensitivity of the closed-loop design to the plant dynamics.

Additional insensitivity to the 18th and 19th design model modes at 3.47 Hz and 3.51 Hz was obtained by including uncertainty representations for these modes as shown in Figure 4. The final uncertainty representation resulted in a controller with sufficient insensitivity to plant variations.

4.3 Final Design Synthesis Model

Figure 6 is a block diagram of the final synthesis model containing the design model, performance objectives, design constraints and uncertainty representations. Weighting functions $w_{s_x}(s)$ and $w_{s_y}(s)$ are constant gains. The weighting functions $w_{r_i}(s)$ are 3rd order transfer functions with magnitude gain shown in Figure 3.

The gain block K_{add} is a diagonal scaling block on the input associated with the additive uncertainty. K_F is a diagonal scaling matrix associated with the uncertainties $\Delta_{F_{18}}$ and $\Delta_{F_{19}}$ on the 18th and 19th mode pole locations. K_{F_u} is a diagonal scaling block

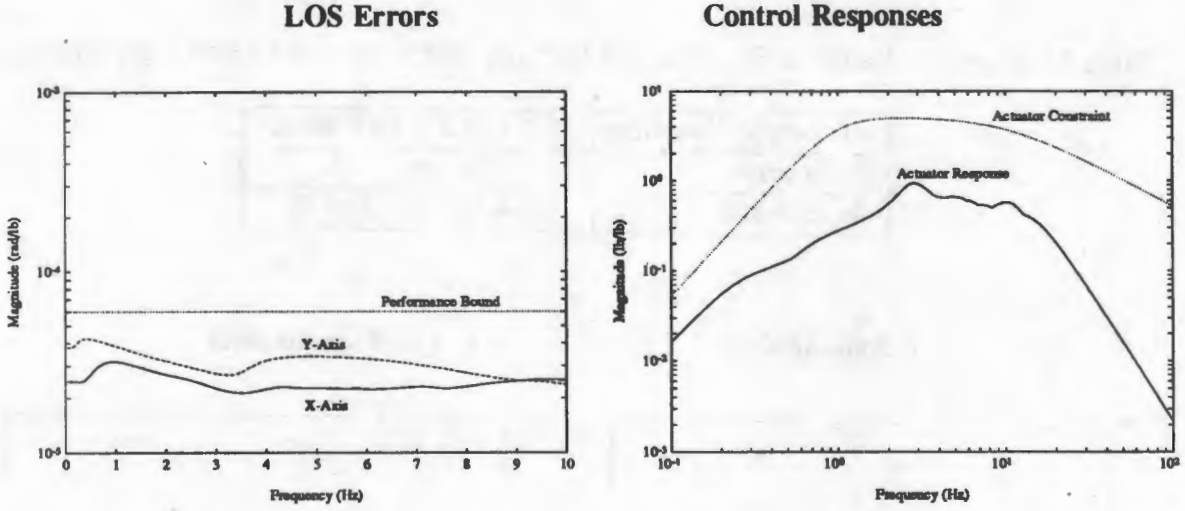

Figure 7: Singular Values of the Closed-Loop Responses to Disturbances.

associated with the feedback uncertainty block Δ_{F_u}.

The design process involves iterating on the selection of the design weightings and scaling gains to obtain a satisfactory trade-off between performance requirements, design constraints and sensitivity to model uncertainties.

The final synthesis model was 86^{th} order, with a w input vector of dimension of 39 and z output vector dimension of 12. The resulting controller was also 86^{th} order. The size of the controller was reduced to the maximum allowable of 58^{th} order using balanced-truncation model reduction.

5 Analysis and Experimental Implementation

Figure 7 shows the closed-loop LOS errors for the X and Y axes and the control responses to disturbances. Vibration suppression is improved over the open-loop system by a factor of 8 in the X axis LOS error and a factor of 5 in Y axis LOS error. The original goal was to achieve a factor of 10 improvement over the open-loop structure. However the initial controller designs were sensitive to the 18^{th} and 19^{th} design model mode locations. The design objective was relaxed to obtain a factor of 5 improvement in LOS error, and to reduce the sensitivity of the closed-loop system to variations in the 18^{th} and 19^{th} modes. Table 1 is a table showing the sensitivity of the closed-loop system to variations in the 18^{th} and 19^{th} mode frequencies for the final design.

The $\mathcal{H}_\infty$ designed controller was discretized using a zero-order-hold approximation, and implemented on a real-time controller running at 280 hz. The closed loop system was excited through the disturbance inputs and the sensor output data recorded. This data was used to reconstruct, off-line, an estimate of the magnitude response from a

Table 1: Allowable Range in Frequency of 18th and 19th Mode For Closed-Loop Stability.

Allowable Variation	18th Mode	19th Mode
% increase	69.5 %	∞
% decrease	78.4 %	90.4 %

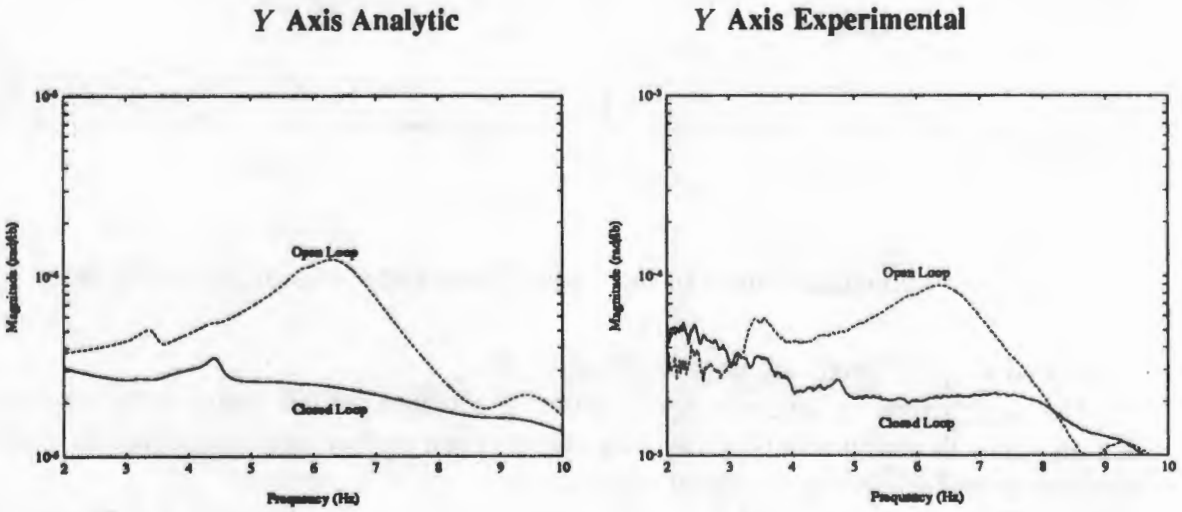

Figure 8: Comparison of Analytic Prediction of Y Axis LOS Error to Experimental Reconstruction.

single disturbance input to the X and Y LOS outputs. Figure 8 compares the analytic prediction and the experimentally reconstructed Y axis LOS error response to a single disturbance. At low frequencies the experimental reconstruction is corrupted by noise due to low amplitude signals with large relative contributions to the LOS error. However from about 3–10 Hz the analytic and experimental results show good agreement. A factor of 5 improvement in LOS error attenuation is seen for the dominant open-loop peak at 6 Hz.

Figure 9 compares the open and closed loop time response of an accelerometer on the structure to a disturbance input. Here the effectiveness of the controller in attenuating disturbances is clearly evident. A low frequency suspension mode (not controlled) is visible in the time response of Figure 9.

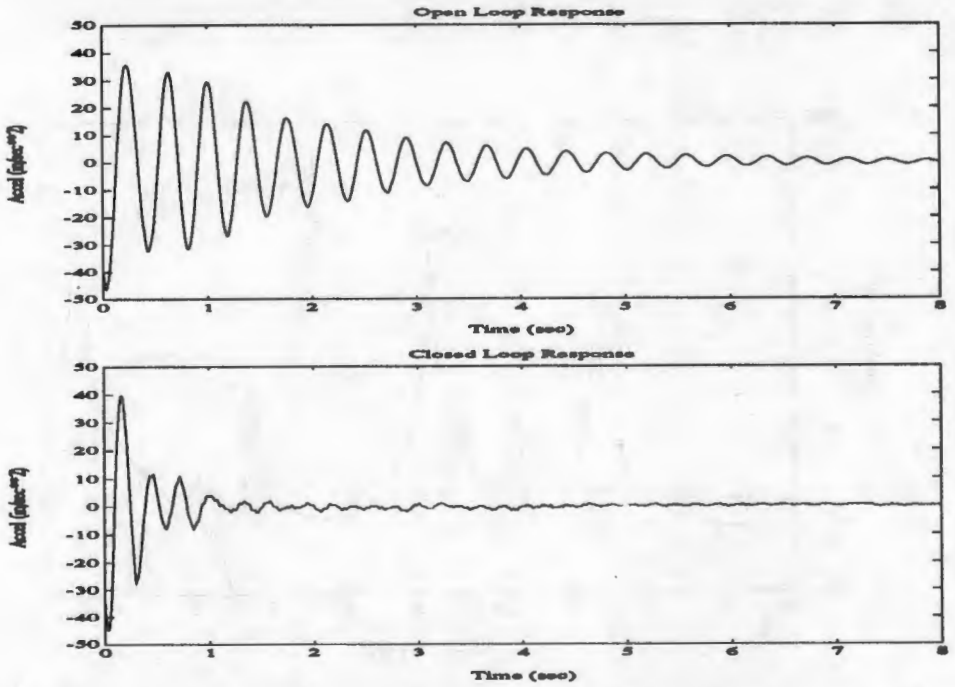

Figure 9: Open and Closed-Loop Time Response of an Accelerometer Output on the DTA Structure to an Impulse Disturbance Input.

6 Contribution of Passive Damping to Control

The DTA structure was designed and constructed with passive damping elements for vibration suppression. Typical LSS designed without passive damping have modal damping ratios significantly less than for the DTA. An analytic study on the contribution of passive damping to the performance of the active control is described in this section.

A representative 'undamped' model of the DTA structure without passive damping was developed based on typical modal damping present in LSS. The active controller was redesigned for the undamped structure using the same design criteria as for the passively damped structure. Comparisons of the passively damped and undamped designs provide a basis for evaluating the importance of passive damping.

6.1 Representative Undamped Structural Model

Modal damping ratios for the DTA structure with passive damping range from 0.023 to 0.121. An analytic model of a DTA structure without passive damping was obtained by reducing the structural mode damping ratios to 0.002, a value determined from measurements of the undamped ring truss component. Modal displacements and frequencies were not changed for the undamped model. Figure 10 is a plot of the maximum singular values of the frequency response from the disturbance inputs to each of the X and Y LOS error outputs.

The frequency response for the undamped model is significantly different from the

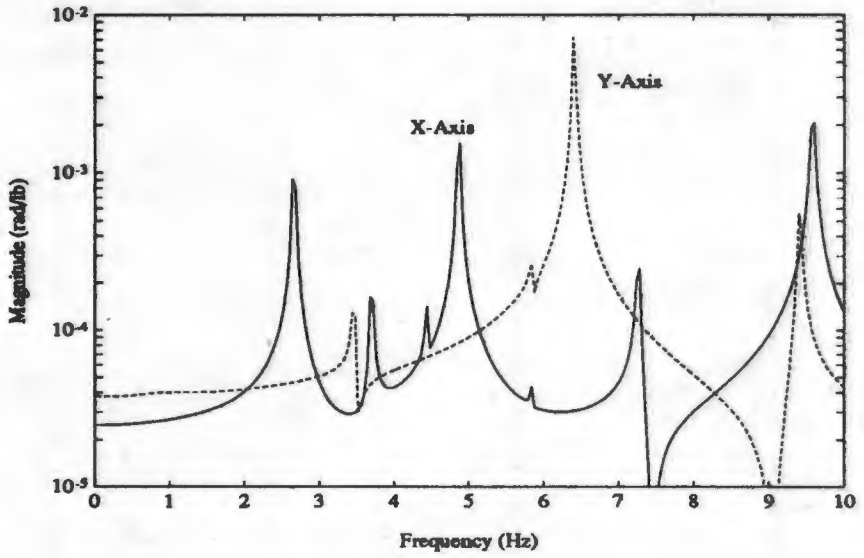

Figure 10: Maximum Singular Values of the Response from Disturbance Inputs to X and Y LOS Error Outputs for the Undamped DTA Model.

DTA model with passive damping (Fig. 2). The undamped model frequency response has many sharp resonance and anti-resonance peaks resulting from the decreased structural damping. In addition, the undamped model shows significant structural response up to 10 Hz whereas the passively damped DTA shows less response at these higher structural frequencies.

6.2 Control Redesign for Undamped Structure

The analytic DTA model without passive damping was used to redesign the $\mathcal{H}_\infty$ controller. With the exception of the DTA plant model, the synthesis model was unchanged from the final $\mathcal{H}_\infty$ control design. Synthesis model weighting functions were the same as in the final design for the passively damped structure.

A sensitivity analysis of the redesigned compensator revealed significantly greater sensitivity to the 18^{th} and 19^{th} design model mode pole locations than for the passively damped system. Table 2 gives a comparison of the allowable independent variations in frequencies for the passively damped system versus the system without passive damping. The passively damped system can tolerate a large increase in the frequency of the 19^{th} mode, while a variation of less than $+1.0\%$ in frequency of the same mode will result in an unstable design for the undamped system.

The $\mathcal{H}_\infty$ compensator resulting from the undamped model had two unstable modes which could not be reduced. Unstable compensators are generally undesireable due to the difficulties in implementation.

Table 2: Mode Frequency Tolerances for Control Designs

Allowable Frequency Variation	18^{th} mode	19^{th} mode
Passively Damped System	$+69.5\%, -78.4\%$	$+\infty, -90.4\%$
Undamped System	$+48.8\% - 77.6\%$	$+0.5\%, -42.0\%$

Controller order reduction for the $\mathcal{H}_\infty$ active controller was affected by the absensce of passive damping in the analytic plant model. Balanced model truncation of the $\mathcal{H}_\infty$ control designs to 58 states resulted in a total magnitude error bound of 0.1628 for the compensator with passive damping compared to 0.2968 for the compensator without passive damping. Reduction of the undamped system compensator to approximately the same total error resulted in a controller with 61 states.

To evaluate the influence of passive damping on controller performance, the $\mathcal{H}_\infty$ controller for the undamped model was redesigned to recover, in part, the sensitivity margins of the $\mathcal{H}_\infty$ controller for the passively damped system. The LOS error performance bound (i.e. $W_S^{-1}(s)$) was relaxed by a factor of two for the undamped DTA model. The uncertainty input gains were increased uniformily to minimize the sensitivity of the undamped closed-loop system to the mode pole locations of the model.

The full-order $\mathcal{H}_\infty$ compensator was 86 states for both the passively damped and undamped DTA models. Figure 11 shows frequency responses to the LOS errors and control feedback from the disturbance inputs for the closed loop full-order design without passive damping. Both the LOS performance and control activities are similar to those of the passively damped system.

The structural mode frequencies of the passively damped and undamped models were perturbed by equal amounts of less than 10% of their nominal values. Figures 12 and 13 show a comparison of the LOS error response to disturbances for both the passively damped and undamped closed-loop systems. Clearly, from Figure 12, the sensitivity of the undamped system is still greater than for the passively damped system. For the same frequency perturbations the passively damped design meets the original performance bound while the undamped design violates even the relaxed performance requirement. The peak response of the LOS error is roughly two orders of magnitude greater for the undamped system as for the passively damped system.

7 Conclusions

An $\mathcal{H}_\infty$ design approach was applied to the active control of a passively damped large space structure test article. Performance objectives, design constraints, and model uncertainties are directly included in the design process. Representation of model uncertainties was used to achieve designs which were insensitive to plant model variations.

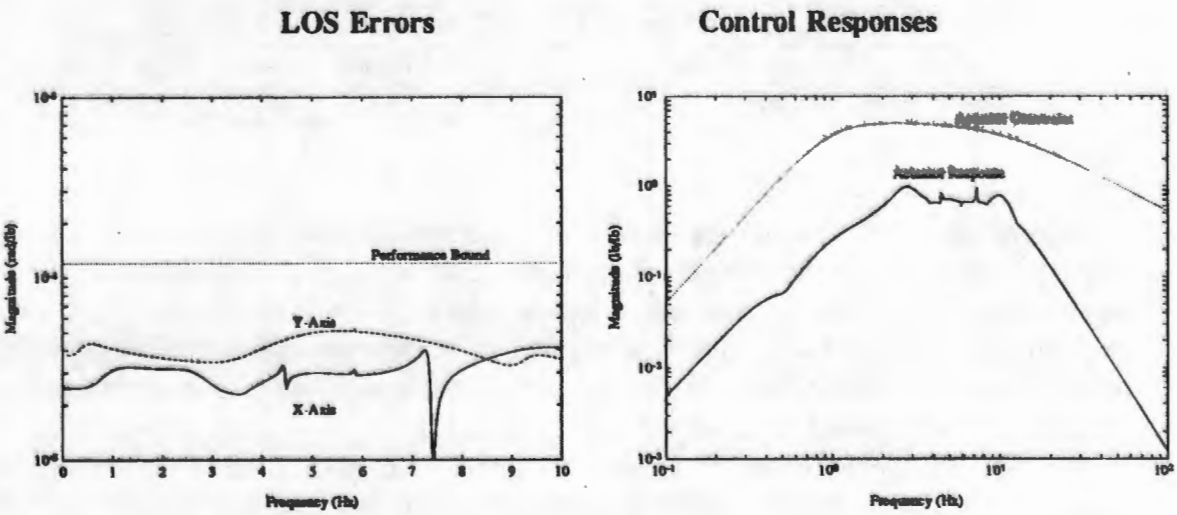

Figure 11: Singular Values of the Closed-Loop Responses to Disturbances for the Undamped $\mathcal{H}_\infty$ Design.

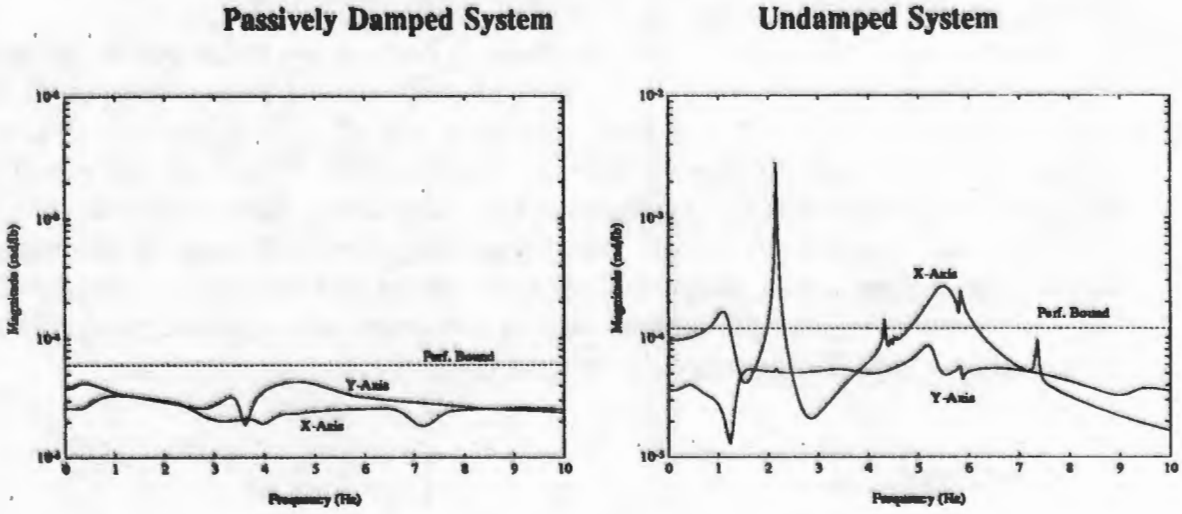

Figure 12: Singular Values of the Closed-Loop Responses to Disturbances for the Passively Damped and Undamped $\mathcal{H}_\infty$ Designs with Perturbed Models.

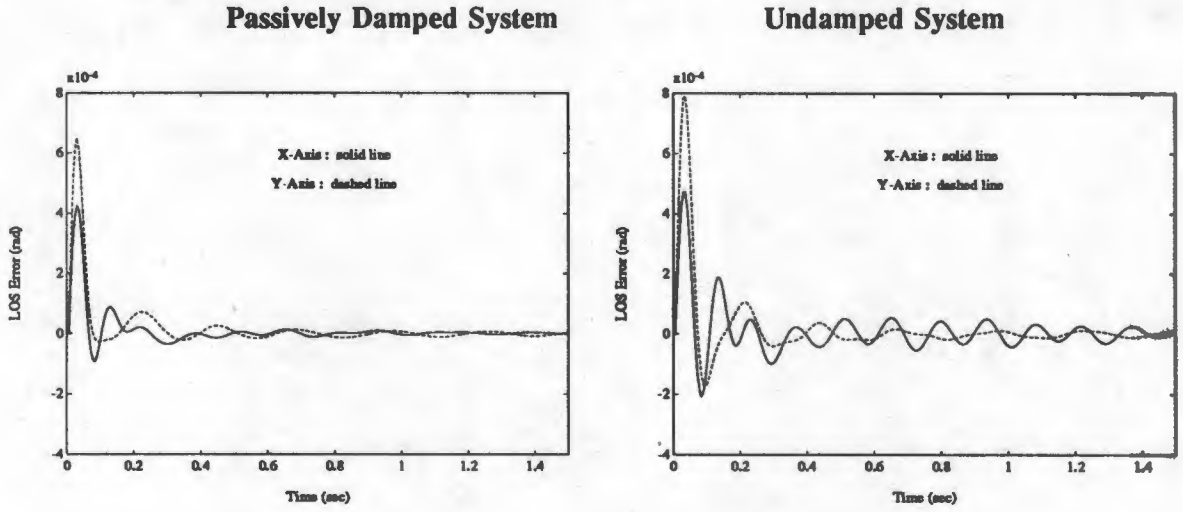

Figure 13: Closed-Loop Time Responses to Disturbances for the Passively Damped and Undamped $\mathcal{H}_\infty$ Designs with Perturbed Model.

Analytical studies into the effects of the passive damping on the active control design reveal that the presense of passive damping decreases the sensitivity of the active controller to model errors and allows for improved performance. Furthermore, active control designs for the passively damped structure were found to be easier to reduce as compared to designs for the model without passive damping.

Hardware implementation of the active control design provided experimental verification of the design results. Analytical prediction showed good agreement to results from the test data.

References

[1] S. Boyd, C. Barratt, and S. Norman. Linear controller design: limits of performance via convex optimization. In *Proc. IEEE, 78(3)*, March 1990.

[2] J.C. Doyle. Structured uncertainty in control system design. In *Proc. 24th IEEE Conference on Decision and Control*, December 1985.

[3] J.M. Maciejowski. *Multivariable Feedback Design.* Addison Wesley, New York, 1989.

[4] M.G. Safonov and D.J.N. Limebeer. Simplifying the $\mathcal{H}_\infty$ theory via loop shifting. In *Proc. 27th Conference on Decision and Control*, December 1988.